

<https://doi.org/10.1038/s43247-024-01961-z>

The Dutch Apollo 11 Goodwill display contains genuine Moon rocks

Check for updates

Thomas André Claude Zillhardt^{1,2,3}✉, Wim van Westrenen⁴, Marianne Nuij⁵, Ryan Warr¹, Zixian Su¹ & Timothy Burnett^{1,3}

In the 1970s, US President Richard Nixon offered moon samples returned by the Apollo 11 and Apollo 17 missions to the leaders of the nations of the World. In this study, we used a combination of advanced X-ray analysis methods, including microtomography, tomosynthesis and hyperspectral chemical mapping to carry out a non-destructive forensic investigation of the Dutch Apollo 11 Goodwill sample, normally on display at the Boerhaave museum in the Netherlands. These powerful methods were uniquely able to non-destructively interrogate the samples encased in plastic without contact, providing 3D images of sample textures and compositional analysis, to assess whether the results agree with archive data on Apollo 11 coarse-grained soil sample number 10085, and to provide new insights on their origins. Our forensic investigation asked the question: were the rocks in the Dutch display actually picked up on the surface of the moon by Neil Armstrong and Buzz Aldrin?

The Moon Sample Return Missions and the Goodwill Lunar Sample Displays

On the 21st of July 1969 at 02:56 UTC, Apollo 11 Commander Neil A. Armstrong set foot on the moon for the first time in the history of humankind. He was quickly followed by Eagle Module pilot Edwin E. “Buzz” Aldrin, and together they spent a few hours on the lunar surface. Their main scientific objective was to scoop surface soil and to collect rock samples. A few weeks after returning to Earth on the 29th of September 1969, they embarked on a 38-day journey with Columbia Module pilot Michael Collins to visit 29 cities in 24 countries¹. As part of this showcase of the American Space Program, 135 Apollo 11 Goodwill Lunar Sample Displays (GLSDs) were gifted to the nations of the World on behalf of US President Richard Nixon. These displays, such as the one pictured in Fig. 1, were based on a uniform design, with a 4 × 6 inch flag (taken to the moon on the same voyage) of the recipient country mounted on a wooden plinth and covered by a plastic slab. At the top of the display, just above the flag, a resin hemisphere encapsulates several small “moon rocks” 2–5 mm in diameter.

In the 1970’s, tracking of museum items was suboptimal, and with time several of these GLSDs, which were presented to individuals rather than institutions, as well as other samples from the moon loaned to international partners, went missing. As of the writing of this article, dozens of Apollo 11 GLSDs are still missing, including those of Cuba, Cyprus, Peru, Vietnam and the United Nations². Investigations led by museums, space artefact hunters, and lawyers managed to recover a number of displays and items, including all of those gifted to the 50 United States of America³. In 2009, a

moon rock given to the former Dutch Prime Minister Willem Drees in 1969 by the US ambassador to the Netherlands, which headlined a national Rijksmuseum exhibit of its ‘oldest artefacts’, was found to be a piece of petrified wood most likely from Arizona⁴. The item, which had been insured for up to \$500,000, is one of many fake moon rocks or displays in circulation. Identification of this sample as a fake was trivial as the item was not embedded in plastic and was relatively large (> 5 cm in diameter), and because testing only required optical and electron microscopy^{5–8}. It is currently kept as a curiosity at the Rijksmuseum under object no. NG-1991-4-25. The same thing cannot be said of the many displays from the Apollo 11 and Apollo 17 missions that went missing, and it is not impossible that the rocks could have been swapped for a replica. To date, none of the approximately 400 displays (including samples distributed to the nations of the world and US states after the Apollo 17 mission) have ever been analysed and no-one has ever managed to prove that the encapsulated rocks are in fact from the moon.

In this paper, we present an original forensic investigation into the Dutch Apollo 11 Goodwill Lunar Sample Display, making use of a combination of non-destructive X-ray imaging techniques. This object, now located in Rijksmuseum Boerhaave in Leiden (the Netherlands), had been reported missing for a number of years before it was officially registered under object number V09113 in 1996⁹. The curators at the Astromaterials Acquisition & Curation Office, part of the Astromaterials Research and Exploration Science (ARES) Division at the Johnson Space Centre (JSC), U.S. National Aeronautics and Space Administration (NASA) have kept a

¹Department of Materials, University of Manchester, Manchester, UK. ²Diamond Light Source, Diamond House: Harwell Science and Innovation Campus, Didcot, Oxfordshire, UK. ³National X-ray Computed Tomography (NXCT), Henry Royce Institute Hub Building, Manchester, UK. ⁴Department of Earth Sciences, Vrije Universiteit Amsterdam, Amsterdam, Netherlands. ⁵Rijksmuseum, Museumstraat 1, Amsterdam, Netherlands. ✉e-mail: thomaszillhardt@cantab.net

Fig. 1 | Dutch Apollo 11 Goodwill plinth with encapsulated moon rocks, flag and presentation sign. Photographies with views from the front (a) and from the side (b).

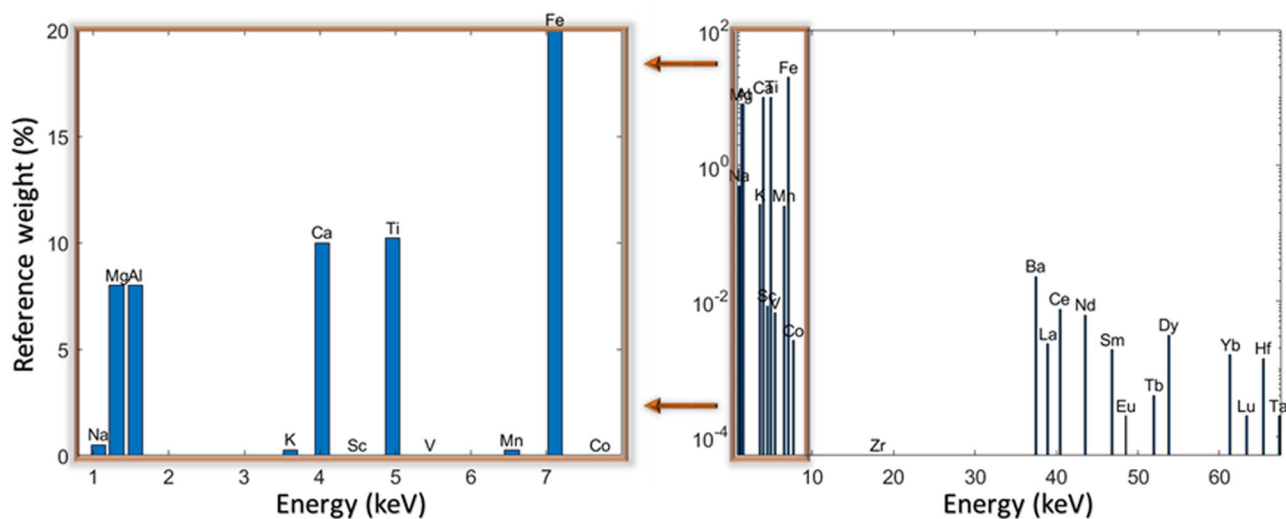
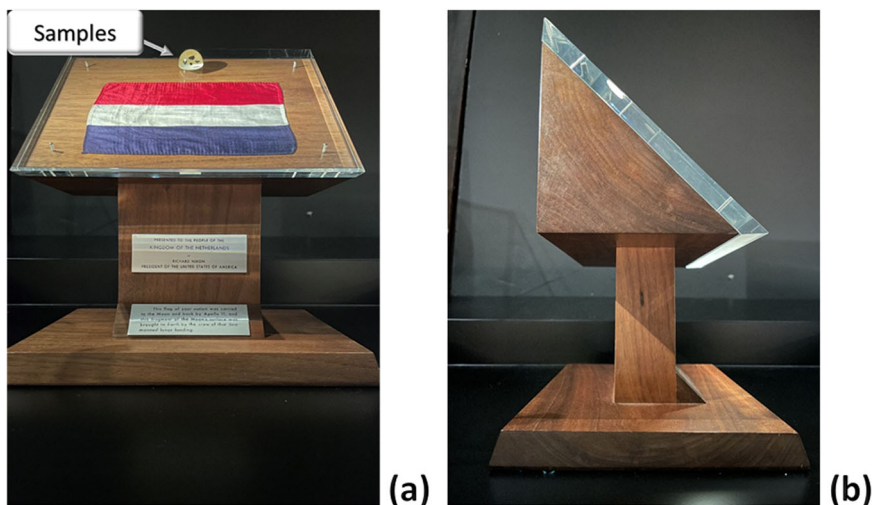


Fig. 2 | Average cation abundances (in wt%) n of moon dust batch no. 10085,11 as a function of K-edge energies: adapted and plotted with data from Beatty et al. ¹⁴, with all the elements on the right, and a magnification focused on low-keV elements on the left. Note that the scale changes from log to normal.

catalogue of samples brought back from the moon and through private communication have indicated that the four fragments inside this display should be part of Apollo 11 sample n°10085,1104¹⁰.

Mineralogy and composition of Apollo 11 sample no. 10085,1104

The Apollo 11 landing site is situated in Mare Tranquillitatis, a major basalt-filled basin near the lunar equator. Basaltic rocks at the landing site likely originated from West Crater, and consist of layers of low- and high-potassium basalts¹¹. A total of ~21.6 kg of samples was collected, consisting of larger basaltic rock samples exposed on the lunar surface, several samples of lunar regolith (the ‘soil’ on the Moon formed by continuous small and large impacts of material onto the surface), and two tube cores sampling the shallow subsurface [12]. Nine scoops taken from the top ~5 cm of the regolith, equalling approximately 10 kg of fine-grained material were added to the larger rock samples in rock box ALSRC no. 1003, apparently in order to prevent excessive bouncing around of the larger samples⁹. Bagged regolith sample 10002, with a composition very similar to the loose material, resided in the same rock box. Back on Earth, part of this regolith material was sieved. The fraction of material smaller than 1 mm in diameter (~ 3.8 kg in total) was numbered sample 10084. The larger particles over 1 mm in diameter constituted sample n°10085 “coarse-fines”; although particles < 1 mm likely

remain in this sample. Subsample no. 10085,11 contains 1227 grains, among which are mafic holocrystalline rock fragments, microbreccia, glass splatter (and agglomerates), irregularly shaped glass, and anorthosite (a plagioclase-rich rock forming the primitive lunar crust and exposed mostly in the lunar highland terrane)¹². Soil breccia (52%) and basalt (37%) were the two most abundant rock types in the sieved samples¹³. Sample no. 10085,1104 is part of this subsample.

The average elemental composition for basalts of sample no. 10085 has been determined by Instrumental Neutron Activation Analysis (INAA) and electron microscopy¹⁴. Figure 2 presents the elemental reference weight as a function of K-edge energy. The sample contains elevated abundances of iron and titanium compared with most Earth basalts, as well as enrichments in lanthanide and actinide trace elements.

In order to assess whether X-ray-based non-destructive techniques could be used to study the encased fragments, the casing material was determined with Raman spectrometry using a Bruker Bravo handheld spectrometer. This showed that the casing consists of Unsaturated Polyester resin (UP) mounted on a poly(methyl methacrylate) (PMMA) plate¹⁵. Both UP and PMMA have a high tolerance to X-ray radiation, with a minimal risk of laboratory X-ray sources causing yellowing at radiation doses orders of magnitude below 30 kGy¹⁶.

Application of X-rays in paleoradiology and geology

The non-destructive aspect of X-ray analysis makes it an exceptional tool for forensics of ancient artefacts as well as (extra)terrestrial materials, especially in cases where the radiation dose is not a detrimental factor. X-ray microtomography (XRM) creates a 3D ‘black and white’ image of the sample based on attenuation of the X-ray beam, which depends for instance on the beam wavelength, relative atomic number, and density of the material. It provides high-resolution 3D images of samples and a virtual replica of the sample that can be explored virtually.

Tomography has previously helped visualise the 3D texture of peralkaline rhyolite volcanic pumice¹⁷, with an image quality sufficient to infer that these fail by brittle fracture. The fragments in the Apollo 11 Dutch display, if authentic, will have originated from a volcanic basin, ‘Mare Tranquillitatis’, which has been the result of a lava flow ejecta from West Crater, containing layers of low- and high-potassium basalts¹¹. Classic petrographic analysis that require the destructive preparation of polished sample thin sections demonstrated that basalt fragments in no. 10085, including 796, 803, 820 and 915, exhibited an antiophitic texture¹⁸, i.e. containing large plagioclase crystals surrounding ilmenite and pyroxene in a poikilitic manner. A previous non-destructive tomography investigation¹⁹ of Apollo 11 sample no. 10057²⁰, a high potassium ilmenite basalt, provided three-dimensional visual observations of characteristic ilmenite (iron-titanium oxide) needles with no preferred orientation inside the sample, as well

as large tabular bundles, and a vesicular texture characteristic of volcanic rocks. This group of high-potassium Apollo 11 basalts with fine-grains and with a high vesicle abundance was termed ‘type A basalts’²¹ with an antiophitic texture¹⁸. The random orientation of ilmenite crystals has more recently been confirmed by three-dimensional X-ray ultramicroscopy (XuM), an SEM-based X-ray transmission technique. It showed that ilmenite crystals ((Fe,Mg)TiO₃) could not only form as the usual plates, but takes varied shapes such as needles²², which can help identify which lava flow the particle originates from. In another recent application of X-ray based techniques, X-ray Computed Tomography (XCT) analysis of Apollo 11, 12, 15, and 17 basaltic samples provided for the first time 3D images of these fragments and found that they were from low-viscosity lavas formed by effusive flows²³.

Prospects of X-ray characterisation in geology

Although XRM/XCT can offer reliable 3D internal views of many specimens, it typically relies on having projections captured over a 180° (parallel beam) or 360° (cone beam) range, which implies either a rotating source-detector assembly (medical imaging) or a rotating sample (industrial imaging). This can prove challenging with unconventional specimens, including with the present case involving a complex object geometry with a small region of interest. Planar Digital Tomosynthesis (PDT) is a new method which allows tomography with no moving parts and no special sample mounting requirements. Radiographs are acquired with an array of multiple in-plane sources to reconstruct limited depth tomography slices using image remapping algorithms²⁴. PDT provides virtual cross section slices within just a few minutes. Although originally designed for mammography²⁵, it is increasingly used in Non-Destructive Imaging (NDT) of electronics²⁶ and aerospace components²⁷, but has not before been used in forensics or geology.

X-ray Hyperspectral Imaging (XHI) is a technique making use of recently developed hybrid pixel photon counting detectors (PCD) able to resolve part of the energy spectrum of the incoming beam. XHI can be used for elemental composition analysis by identifying energy absorption K-edges. The latter represent a rapid photoelectric absorption when the X-ray energy is just above the binding energy of the K-shell electrons giving a characteristic material-specific signal. These detectors make use of the electron-hole cloud generated (photoelectric) by photon hits on specific semiconductor sensor materials to create a signal (direct conversion). This is then transmitted to an ASIC (application-specific integrated circuit) by bump-bonding of the pixels to the sensor, to be processed by each pixel



Fig. 3 | Close-up photograph of the four moon rocks: the four rocks are numbered by distance from the bottom of the dome, 1 being the closest. The diameter of the plastic dome is approximately 2.5 cm.

Fig. 4 | Reconstructed digital tomosynthesis slices (saturated) from the dome. Views of plinth laying down (a), and on its left side (b), showing virtual sections from bottom (i) to top (iii) of the dome. The slices are distanced by about 0.03 inches or 0.8 mm.

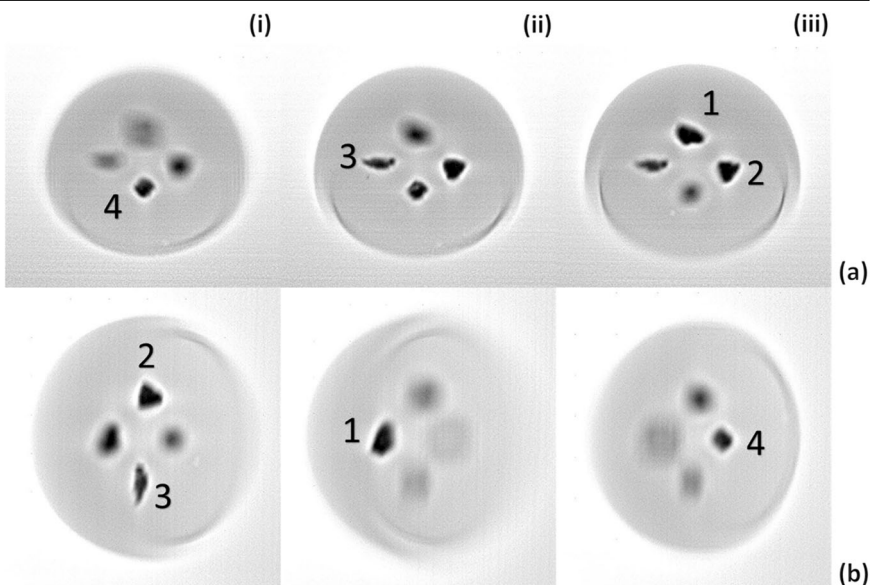
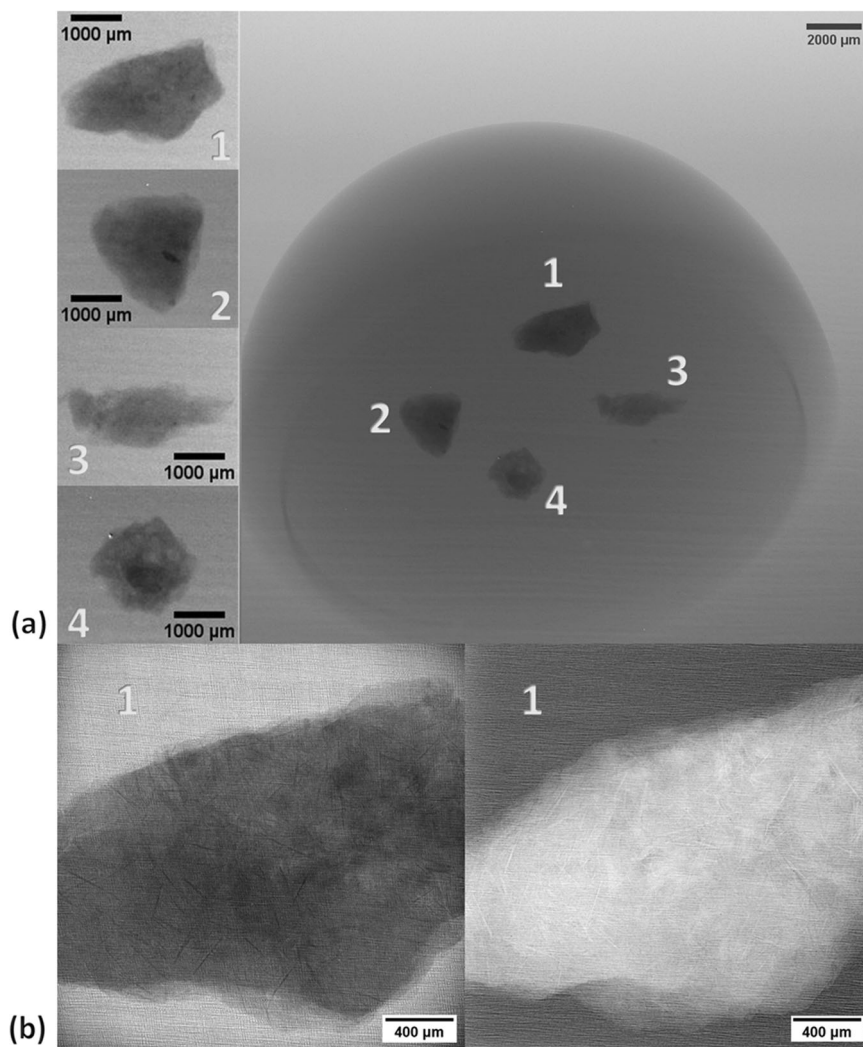


Fig. 5 | Radiography projections of the hemisphere. Views with the four fragments (a) numbered from 1 to 4, and high-resolution projections of the fragment no. 1 (b) in transmission (left) and absorption (right).



circuitry. The Timepix 3 (TPX3) ASIC^{28,29} is a direct pixel-readout detector based on simultaneous Time of Arrival (ToA) and Time over Threshold (ToT). When a photon hits the sensor and initiates a charge at the bump bond interface, a 4-bit counter records the ToA and a 14-bit overflow counter counts as long as the charge is over the minimum threshold providing the ToT. The Medipix/Timepix family of chips, developed by CERN, have been used to determine the material composition of paintings³⁰ as well as in drill cores used in mining inspection^{31,32}. In this experiment, both ASICs were bump-bonded to a 1 mm thick Cadmium-Telluride (CdTe) sensor providing very good energy sensitivity in the 5–500 keV range and acceptable energy resolution (HEXITEC 1 keV at 60 keV, TPX3 3–5 keV at 60 keV). These detectors can provide absorption radiographs for each spectral band or bin instead of an integral image, and because a specific element can absorb more at a known energy value, it is possible to infer the elemental composition of the material studied.

First observations

Visual observation of the moon rocks in the GLSD indicated that they were unlikely to be glass or micro-breccia, due to the lack of amorphous texture and their dark colour. A macro view of the samples in the plastic hemisphere is presented in Fig. 3, within the wooden plinth visible underneath. Each rock is identified with a single digit number from the top of the plinth.

Figure 4 presents selected reconstructed slices from three different scans corresponding to the three sample orientations in the tomosynthesis scanner. They give an idea of the relative positions of the rocks in the plastic, their shapes and their three-dimensional spacing. In particular, it was noted

that a few specific angular views allowed for unique observation where the stones do not overlap when viewed from a single perspective, either because they are not at the same height or because there is sufficient space between two other rocks. Note that these images have been saturated to better observe the edges of the stones.

The four fragments have different shapes, but all dimensions are below 3 mm in length. The DT virtual slices provided positional information in less than 50 s and have been essential in determining the best course of action for subsequent analyses, including relative positions and rock dimensions have allowed. Multiple sample positioning, which would not have otherwise been possible with XCT, showed that the encapsulation hemisphere was even and had a dual-layer encasement.

Results

Phase morphology of the rock fragments by 3D micro-tomography and segmentation

The macro-resolution projection of the Unsaturated Polyester resin (UP) hemisphere with the four rock fragments presented in Fig. 5a provides initial information on the microstructural features that are observable in the material. In particular, highly attenuating particles are visible in fragments 2 and 4 (at these projection angles), and less attenuating regions in fragments 1, 2, and 4 are indications for the presence of porosity. Figure 5b, which shows the high-resolution projections of fragment 1, presents similar attenuation differences, but also shows the presence of needle-like features. These needles appear to present a thickness range of about 13–19 µm and do not seem to share any common orientation or length.

Fig. 6 | Tomography 3D volume visualisation and rendering. Macro-resolution virtual segmentation (a) and reconstructed slice (b), and high-resolution reconstructed slice of fragment 1 (c) with horizontal (i) and vertical slice (ii).

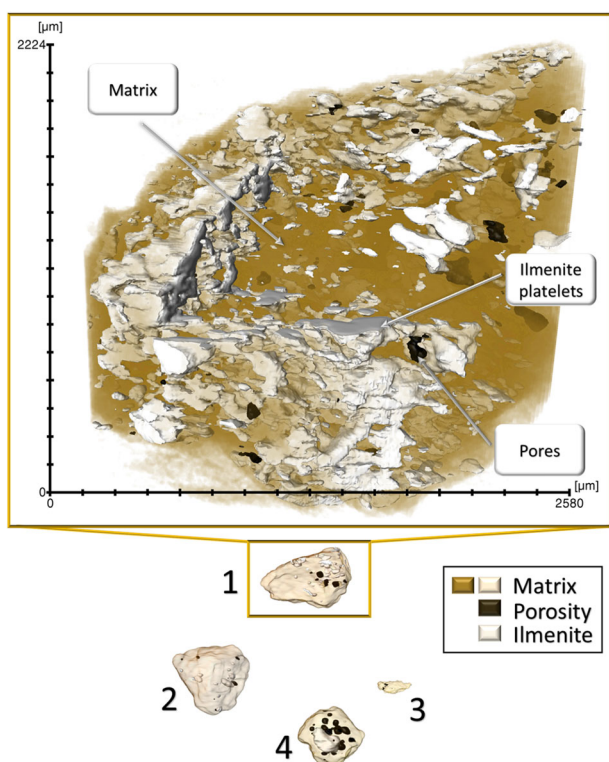
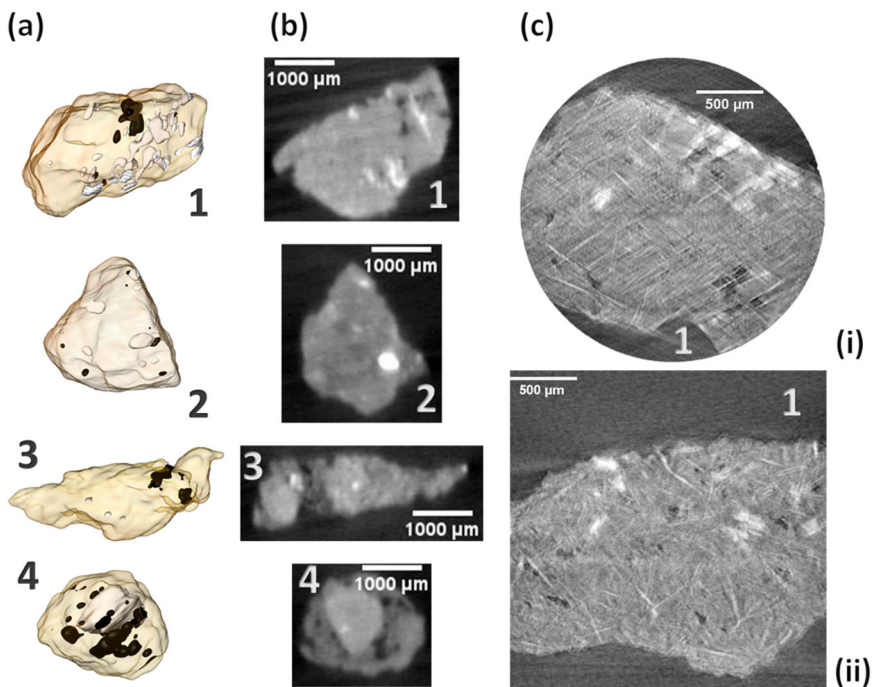


Fig. 7 | Three-dimensional segmentation view of fragment 1: high-resolution tomography (with cut-out volume to inspect internal features), and its location in the macro-resolution tomography, showing a transparent matrix highlighting the internal pores and higher density ilmenite.

Reconstructed tomograms are presented in Fig. 6, as segmented visualisations (a), virtual sections (b) for the macro-tomography, and slices (c) for the high-resolution tomography. Images (a) and (b) provide evidence of connected porosity and large dense regions, especially in particle 4 where a large high density region can be observed in its centre. By zooming into the high-resolution tomography of Fig. 6c, needle-shaped features can be

observed. Once segmented, as presented in Fig. 7, it can be seen that these needles are actually plates and concatenations of plates. They have seemingly random orientations and varying shapes, and some seem to have been fractured into smaller plates. The edges are sharp, testifying a legacy of catastrophic fracture and a lack of erosion.

Label analysis of the segmented volumes provides a quantification of the phases identified in the datasets. As presented in Table 1, three phases have been identified, of which the matrix is the main constituent. Pores make up only ~2% of the total volume on average, with an important difference for the 4th fragment at 4.9%. The latter also contains 9.7% of highly attenuating phases, which is more than the average of 3.6%, and is mostly explained by the large mass in its centre.

The high-resolution X-ray CT scans offer complementary information, by being able to identify needle-like features, which have been labelled as the same dense material. The matrix occupies almost 80% of the total volume, while pores and plates are 1.8% and 18.4% of the 3D segmented dataset respectively. This tends to show, when comparing the macro-scan for fragment n°1 and its high-resolution equivalent, that more than half the pores were smaller than the 22.27 µm/pixel of the macro-scan. Similarly, it appears that about 81% of the dense material is spaced platelets.

Material composition characterisation with hyperspectral X-ray imaging

The GLSD was mounted on its side so that the line of sight allowed the transmission of X-rays through just one rock fragment at a time (preventing overlapping of signals). X-ray Hyperspectral Imaging (XHI) imaging results are shown in the graph of Fig. 8. With flat-field correction, denoising and dark pixel removal, the spectral dataset provided a spectrum at each pixel position with an energy accuracy of about 2 keV. The rock fragments are on the top-right side of the frame, and the figure shows an integral image (summing the spectrum), a coloured image (through allocating RGB channels to parts of the spectrum), and the locations where spectrum profiles were extracted with a 3-pixel radius. Whilst the background is mostly flat, the two positions inside the samples presented in Fig. 8 indicate the presence of elements in the lanthanide series, and in particular barium and samarium. Flat field correction and background normalization helped highlight these heavy elements, however statistics are poorer in the 4 to 5 keV range due to fewer counts and further analysis was required.

Principal Component Analysis (PCA) which has been previously applied to hyperspectral data from photon counting detectors³³ and is particularly well-adapted to noisy spectral data was used to identify different phases. Using the eigen values decomposition method we have calculated the coefficients of the first four principal components, and from them their corresponding ‘eigen’-images. Figure 9a essentially shows that the first component is the mean signal which is saturated by noise as expected, but more interestingly shows the three other components as potentially corresponding to the identification of specific (sets of) elements in the samples. PC2 most likely shows the combined effect of the presence of high K-edge energy elements to which the detector is sensitive but where the X-ray flux is lowest, and PC3 and PC4 provide evidence of high concentrations of iron and titanium. In each case the eigen-images indicate that the effect observed comes directly from the sample. In order to improve confidence in the results, a slightly different variant of this method has also been tested, Maximum noise fraction transform (MNF), which is particularly efficient in more noisy datasets³⁴. This can provide non-adjusted principal components arranged in order of image quality, allowing to clearly identify the signal underneath the noise as seen in Fig. 9b. Similarly, both titanium and iron are identified.

Discussion: The Origins of the Rocks in the Goodwill Display

The size of the Apollo GLSD, the inability to disassemble it and the embedding of the moon rock samples, meant that special non-destructive methods had to be employed. Microtomography has provided evidence of needle-like features and tabular bundles as observed before¹⁹, and three-dimensional

visualisation through segmentation demonstrated that many of these features are plates. This corroborates previous observations²², and the vesicular texture is consistent with rocks formed due to volcanic activity, as observed on a closely related batch of samples²³. This is because these features are the characteristic signature of ilmenite (FeTiO₃) sheets, and it has been shown in other lunar samples that high modal abundances (9–19%) are most often found in moon samples³⁵. The dimensions of the grains also match those found in other Apollo sample batches³⁶.

Hyperspectral material composition identification has hinted at the presence of high concentrations of both titanium and iron, which are major constituents of ilmenite crystals found in lunar basalts, and which are known to be present in high abundances in Apollo sample 10085 (~10 wt% TiO₂ and ~20 wt% FeO in basalt fragments, e.g. Beatty et al.¹⁴). Further, lanthanides such as lanthanum and samarium, which are enriched in many near-side lunar basalt samples compared to average terrestrial basalts³⁷ have also been detected in at least two of these fragments using XHI. Overall, the textural, mineralogical, and chemical evidence is all consistent with these samples being derived from Apollo sample 10085, and therefore of lunar origin.

Conclusions

Non-destructive analysis of the Dutch Apollo 11 Goodwill Lunar Sample Display was performed using digital tomosynthesis, high-resolution X-ray computed tomography, advanced image reconstruction methods, and hyperspectral X-ray imaging, providing quantitative data regarding specific compositional features of the specimens, with elemental sensitivity similar to EDX in EM. The presence of elements from the lanthanide family as well as the noticeable detection of high titanium and iron contents support an Apollo 11 landing site origin of the rocks. Current methodology drawbacks include imaging time, pixel size, magnification and sensitivity to large energy range. The imaged textures in the rock fragments confirm their volcanic origin and the ilmenite-bearing mineralogy are fully consistent with the chemical information. Together with their embedding in the Goodwill sample plaque make it extremely likely these are genuine moon rock samples—and certainly exclude the theory that it may be petrified wood. This correlative multi-modality technique and characterisation

Table 1 | Label analysis for the macro-scan, units are in vol%

Materials	Fragment 1	Fragment 2	Fragment 3	Fragment 4
High density	3.4%	1.0%	0.4%	9.7%
Matrix	95.7%	98.6%	98.1%	85.4%
Pores	0.8%	0.4%	1.5%	4.9%

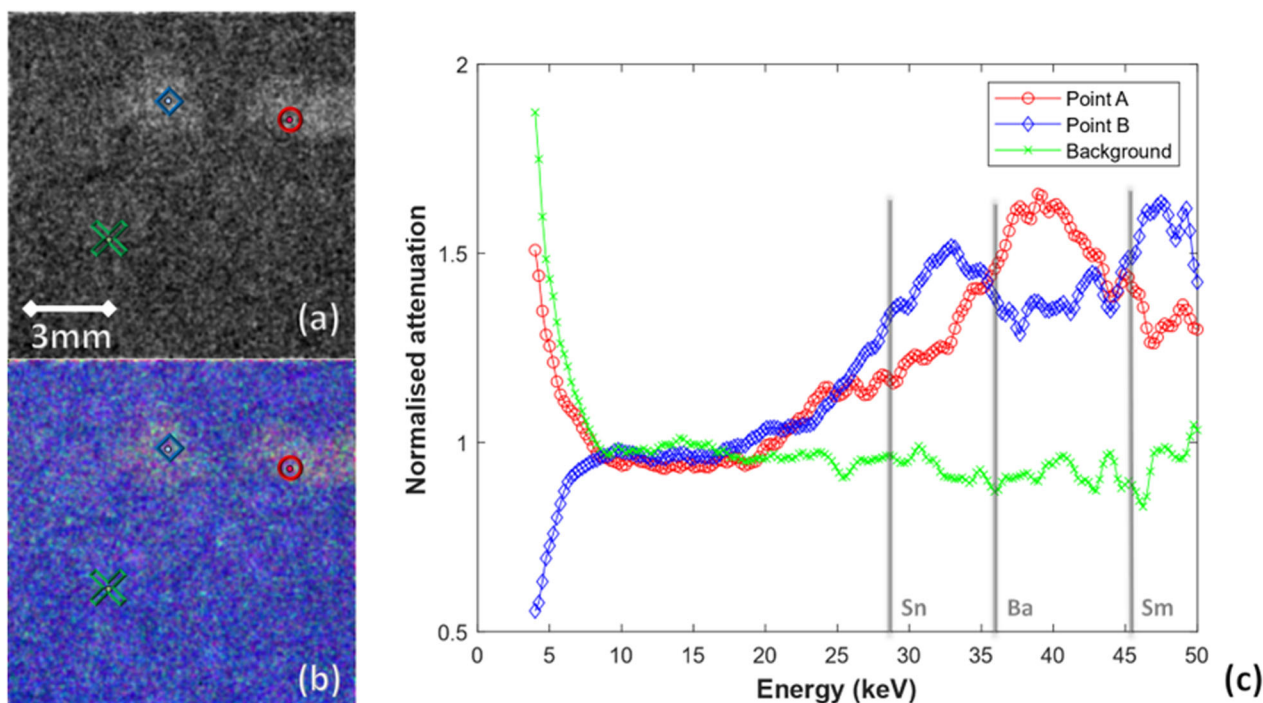


Fig. 8 | Hyperspectral imaging signal. Summed image (a), spectral band-coloured image (b) and spectrum at the dotted locations with a 3-pixels neighbourhood size (c). Cross, circle, and diamond markers in (a) and (b) refer to the corresponding per-pixel (with 3-pixel neighbourhood size) spectrum in (c).

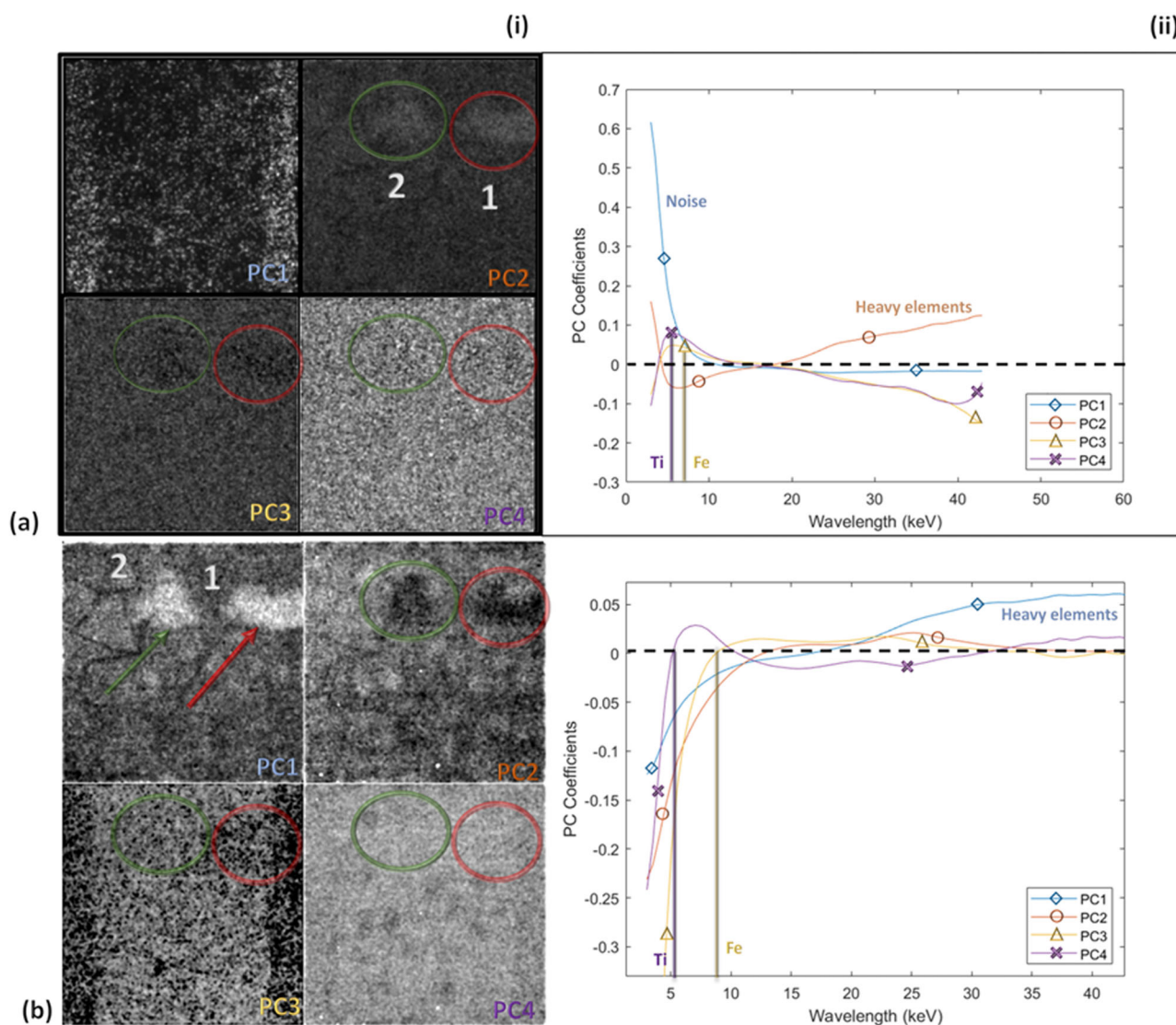


Fig. 9 | Processed hyperspectral data for material characterisation. Principal component analysis (a) and maximum noise fraction transform analysis (b) with principal bands (i) and principal component coefficients plots (ii). A coefficient above 0 indicates similarity. Red and green circles/arrows in (i) define two different rocks.

workflow showcases advanced non-destructive capabilities for the study and forensic investigation of both highly valuable samples and specimens with potential biohazard which can remain contained during scanning.

Methods

X-ray tomography and tomosynthesis

The wide-field tomosynthesis was acquired on an Adaptix® XYP scanner with a 50 keV W-target X-ray source with a current of 200 μ A over a 500 ms exposure per projection and 49 projections; details on this modality are available in Supplementary Fig. 1. The low- and high-resolution tomograms were collected on a Zeiss Xradia 620 X-ray microscope with a macro ($\times 0.4$) scintillator and microscopic lens ($\times 4$) respectively, a pixel size of 22.7 μ m and 2.37 μ m (final, after binning). Both used an acceleration voltage of 112 kV and binning 2. Experimental setup pictures and a summary table are available in details on this modality are available in Supplementary Fig. 2 and Supplementary Table 1, respectively.

Hyperspectral imaging

The X-ray cone beam was provided by a Nikon W-source set at 80 kV and 70 μ A. The Timepix3 detector mounted with a 1 mm CdTe sensor was positioned 70 mm away from the plastic hemisphere (see Supplementary

Fig. 3). The energy was calibrated with a 370 MBq Am^{241} X-ray source fitted with Mo, Tb and Ba fluorescence plates. The Timepix3 was set to acquire in Time-over-Threshold with a full-spectrum capability, and pixel clustering. A low energy cut-off was set to 4 keV and the data was binned into images with a step size of 0.25 keV and an energy spread of 2.5 keV.

Data availability

Raw data has been published online and can be freely accessed online³⁸, no access code is required (DOI: 10.48420/27653688). This repository contains the tomography projections for X-ray CT, from which the volumes can be reconstructed, the pixel-hit files from the spectroscopic acquisition, and a Matlab database containing processed spectroscopic data.

Code availability

The code used in this project can be accessed: 1. Through the CCPI-CIL Imaging Library for the tomography reconstruction. 2. By request to the corresponding author for the hyperspectral analysis. CT segmentation was performed in Avizo 2020.3.

Received: 14 January 2024; Accepted: 11 December 2024; Published online: 28 December 2024

References

- Uri, J. 50 Years Ago: Apollo 11 Astronauts Return from Around the World Goodwill Tour. (ed Mars K). NASA Johnson Space Center (2019).
- Lefkow, C. What happened to the Apollo goodwill moon rocks? Preprint at <https://phys.org/news/2019-06-apollo-goodwill-moon.html>, <https://phys.org/news/2019-06-apollo-goodwill-moon.html> (2019).
- Eversley, M. Former NASA agent toils to find missing moon rocks (2012).
- Sterling, T. 'Moon rock' in museum is just petrified wood. (NBC News (2022)).
- Bouquet, M. *Museums: A Visual Anthropology*. Bloomsbury Publishing (2013).
- Pol, Bvd. *Fly me to the moon: a project by Bik van der Pol*. Sternberg Press (2007).
- Edwards, L. Moon Rock Turns Out to be Fake. Phys.org (2009).
- Rijksmuseum. Steen, door Drees ontvangen van de Amerikaanse ambassadeur, voor 1969 - Rijksmuseum. Rijksmuseum (2023).
- Huisman, T., Maas, A. & Mass, A. C. *Knappe koppen - geschiedenis van de wetenschap in Nederland*. Uitgeverij WBOOKS (2013).
- Zeigler, R. A. Apollo 11 Goodwill Lunar Display "moon rocks". (ed Zillhardt TAC). NASA (2022).
- Beaty, D. W. & Albee, A. L. The geology and petrology of the Apollo 11 landing site. *Lunar Planet. Sci. Conf. Proc.* **1**, 23–35 (1980).
- King, E. A., Carman, M. F. & Butler, J. C. Mineralogy and petrology of coarse particulate material from lunar surface at tranquillity base. *Science* **167**, 650–652 (1970).
- Wood, J. A., Marvin, U. B., Powell, B. N. & Dickey, J. S. Mineralogy and Petrology of the Apollo 11 Lunar Sample. *SAO Special Report* **307**, (1970).
- Beaty, D., Hill, S. M., Albee, A. L., Ma, M. S. & Schmitt, R. A. The petrology and chemistry of basaltic fragments from the Apollo 11 soil - I (1979).
- Heijna, M. C. R., de Groot, S. & Vreeling, J. A. Comparison of irradiation behaviour of HTR graphite grades. *J. Nucl. Mater.* **492**, 148–156 (2017).
- Aquino, K. A. S., Araújo, E. S. & Guedes, S. M. L. Influence of a hindered amine stabilizer on optical and mechanical properties of poly(methyl methacrylate) exposed to gamma irradiation. *J. Appl. Polym. Sci.* **116**, 748–753 (2010).
- Hughes, E. C., Neave, D. A., Dobson, K. J., Withers, P. J. & Edmonds, M. How to fragment peralkaline rhyolites: observations on pumice using combined multi-scale 2D and 3D imaging. *J. Volcanol. Geotherm. Res.* **336**, 179–191 (2017).
- Grove, T. L. & Beaty, D. W. Classification, experimental petrology and possible volcanic histories of the Apollo 11 high-K basalts. *Lunar Planet. Sci. Conf. Proc.* **1**, 149–177 (1980).
- Jones, J. S. & Garvin, J. X-ray Computed Tomography of Tranquility Base Moon Rock. In: *Lunar And Planetary Science And Exploration*. NASA Goddard Space Flight Center (2019).
- Administration NAS. *Lunar Sample Compendium*. CreateSpace Independent Publishing Platform (2018).
- The Lunar Sample Preliminary Examination T. Preliminary Examination of Lunar Samples from Apollo 11. *Science* **165**, 1211–1227 (1969).
- Kiely, C., Greenberg, G. & Kiely, C. J. A New Look at Lunar Soil Collected from the Sea of Tranquility during the Apollo 11 Mission. *Microsc. Microanal.* **17**, 34–48 (2011).
- Gawronska, A. J., McLeod, C. L., Blumenfeld, E. H., Hanna, R. D. & Zeigler, R. A. New interpretations of lunar mare basalt flow emplacement from XCT analysis of Apollo samples. *Icarus* **388**, 115216 (2022).
- Soloviev, V. Y., Renforth, K. L., Dirckx, C. J. & Wells, S. G. Meshless reconstruction technique for digital tomosynthesis. *Phys. Med. Biol.* **65**, 085010 (2020).
- Grant, D. G. TOMOSYNTHESIS: a three-dimensional radiographic imaging technique. *IEEE Trans. Biomed. Eng.* **BME-19**, 20–28 (1972).
- Roh, Y. J., Park, W. S. & Cho, H. Correcting image distortion in the X-ray digital tomosynthesis system for PCB solder joint inspection. *Image Vis. Comput.* **21**, 1063–1075 (2003).
- Rebuffel, V. & Pires, S. R. Automatic delamination defects detection in radiographic sequences of rocket boosters (2003).
- Poikela, T. et al. Timepix3: a 65K channel hybrid pixel readout chip with simultaneous ToA/ToT and sparse readout. *J. Instrum.* **9**, C05013–C05013 (2014).
- Frojd, E. et al. Timepix3: first measurements and characterization of a hybrid-pixel detector working in event driven mode. *J. Instrum.* **10**, C01039–C01039 (2015).
- Zemlicka, J. et al. Analysis of painted arts by energy sensitive radiographic techniques with the Pixel Detector Timepix. *J. Instrum.* **6**, C01066 (2011).
- Luth, S. et al. Building 3D geomodels using XRF-XRT-generated drill core data: The Lovisa-Håkansboda base metal- and Strassa-Blanka iron deposits in Bergslagen, Sweden. In: *15th SGA Biennial Meeting on Life with Ore Deposits on Earth, AUG 27–30, 2019, Univ Glasgow, Glasgow, SCOTLAND*. SOC GEOLOGY APPLIED MINERAL DEPOSITS-SGA (2019).
- Cioacă, M.-E. et al. Mineralogical Setting of Precious Metals at the Assarel Porphyry Copper-Gold Deposit, Bulgaria, as Supporting Information for the Development of New Drill Core 3D XCT-XRF Scanning Technology (2020).
- Egan, C. K., Jacques, S. D. M. & Cernik, R. J. Multivariate analysis of hyperspectral hard X-ray images. *X-Ray Spectrometry* **42**, 151–157 (2013).
- Green, A. A., Berman, M., Switzer, P. & Craig, M. D. A transformation for ordering multispectral data in terms of image quality with implications for noise removal. *IEEE Trans. Geosci. Remote Sens.* **26**, 65–74 (1988).
- Heiken, G. H. & Vaniman, D. T. Characterization of lunar ilmenite resources. *Lunar Planet. Sci. Conf. Proc.* **20**, 239–247 (1990).
- Xue, Z., Welsh, D. F., Neal, C. R. & Xiao, L. Understanding the textures of Apollo 11 high-Ti mare basalts: A quantitative petrographic approach. *Meteoritics Planet. Sci.* **56**, 2211–2229 (2021).
- Gale, A., Dalton, C. A., Langmuir, C. H., Su, Y. & Schilling, J.-G. The mean composition of ocean ridge basalts. *Geochem. Geophys. Geosyst.* **14**, 489–518 (2013).
- Zillhardt, T. A. C., Westrenen, W. v., Nuij, M., Warr, R., Burnett, T. L. Data: The Forensics of the Dutch Apollo 11 Goodwill Moon Rocks Using Advanced X-ray Imaging and Spectroscopy. X-ray images. <https://doi.org/10.48420/27653688> (2023).
- Oke, E. 2020. Transforming Tissue Differentiation via Quantum Digital Tomosynthesis. Innovate UK. £1,376,669. 106175. <https://gtr.ukri.org/projects?ref=106175#/tabOverview>.

Acknowledgements

The authors are grateful for experimental beamtime awarded by the NXCT at Manchester. They also would like to thank the Rijksmuseum for facilitating this investigation and NASA for helpful discussions, especially Dr Ryan A. Zeigler. This work was supported by the National Research Facility for Lab X-ray CT (NXCT) through EPSRC grant EP/T02593X/1. Hyperspectral imaging was made possible by Innovate UK under funding grant number #106175 'Transforming Tissue Differentiation via Quantum Digital Tomosynthesis'³⁹. This project was made possible with funding from IDTV Netherlands (Historisch Bewijs: de Maansteen van Boerhave [Historical Evidence: the Moon rock of Boerhave Museum]).

Author contributions

T.Z.: Investigation, Writing - Original Draft, Formal analysis, Methodology, Software, Data Curation, Visualization. Wim van Westrenen: Writing - Review & Editing. M.N.: Investigation, Resources. R.W.: Investigation. Z.S.: Investigation. T.B.: Conceptualization, Methodology, Funding acquisition, Supervision, Writing - Review & Editing.

Competing interests

The authors have no conflicts of interest to declare. All co-authors have seen and agree with the contents of the manuscript and there is no financial interest to report. We certify that the submission is original work and is not under review at any other publication.

Additional information

Supplementary information The online version contains supplementary material available at <https://doi.org/10.1038/s43247-024-01961-z>.

Correspondence and requests for materials should be addressed to Thomas André Claude Zillhardt.

Peer review information *Communications Earth & Environment* thanks the anonymous reviewers for their contribution to the peer review of this work.

Primary Handling Editor: Joe Aslin. A peer review file is available

Reprints and permissions information is available at <http://www.nature.com/reprints>

Publisher's note Springer Nature remains neutral with regard to jurisdictional claims in published maps and institutional affiliations.

Open Access This article is licensed under a Creative Commons Attribution 4.0 International License, which permits use, sharing, adaptation, distribution and reproduction in any medium or format, as long as you give appropriate credit to the original author(s) and the source, provide a link to the Creative Commons licence, and indicate if changes were made. The images or other third party material in this article are included in the article's Creative Commons licence, unless indicated otherwise in a credit line to the material. If material is not included in the article's Creative Commons licence and your intended use is not permitted by statutory regulation or exceeds the permitted use, you will need to obtain permission directly from the copyright holder. To view a copy of this licence, visit <http://creativecommons.org/licenses/by/4.0/>.

© The Author(s) 2024